Cerebral Cortex March 2007;17:732-741
doi:10.1093/cercor/bhk025
Advance Access publication April 28, 2006

High-Frequency Activity in Human Visual Cortex Is Modulated by Visual Motion Strength

Markus Siegel[1,2], Tobias H. Donner[1,2], Robert Oostenveld[2,3], Pascal Fries[2,4] and Andreas K. Engel[1]

[1]Department of Neurophysiology and Pathophysiology, Center of Experimental Medicine, University Medical Center Hamburg-Eppendorf, University of Hamburg, 20246 Hamburg, Germany, [2]F.C. Donders Centre for Cognitive Neuroimaging, Radboud University Nijmegen, 6525 EN Nijmegen, The Netherlands, [3]Center for Sensory-Motor Interaction, Aalborg University, 9220 Aalborg, Denmark and [4]Department of Biophysics, Radboud University Nijmegen, 6525 EZ Nijmegen, The Netherlands

A central goal in systems neuroscience is to understand how the brain encodes the intensity of sensory features. We used whole-head magnetoencephalography to investigate whether frequency-specific neuronal activity in the human visual cortex is systematically modulated by the intensity of an elementary sensory feature such as visual motion. Visual stimulation induced a tonic increase of neuronal activity at frequencies above 50 Hz. In order to define a functional frequency band of neuronal activity, we parametrically investigated which frequency band displays the strongest monotonic increase of responses with strength of visual motion. Consistently in all investigated subjects, this analysis resulted in a functional frequency band in the high gamma range from about 60 to 100 Hz in which activity reliably increased with visual motion strength. Using distributed source reconstruction, we found that this increase of high-frequency neuronal activity originates from several extrastriate cortical regions specialized in motion processing. We conclude that high-frequency activity in the human visual motion pathway may be relevant for encoding the intensity of visual motion signals.

Keywords: area MT, gamma band, MEG, motion discrimination, oscillation, synchronization

Introduction

A fundamental building block for our understanding of the functional role of any parameter of neural activity in sensory coding is to know if this parameter is monotonically related to the intensity of stimulus features. Although such stimulus–response functions have extensively been studied for single-neuron firing rates, such a relationship has yet hardly been investigated for measures of neuronal population activity such as the local field potential (LFP), the electroencephalogram, or the magnetoencephalogram (MEG). Particularly, population activity in the gamma band (>30 Hz) has attracted strong interest during recent years and has been implicated in various specific aspects of cortical processing, such as binding of distributed representations (Eckhorn and others 1988; Gray and others 1989; Lutzenberger and others 1995; Singer and Gray 1995; Tallon-Baudry and Bertrand 1999), attentional modulation of sensory signals (Niebur and Koch 1994; Gruber and others 1999; Steinmetz and others 2000; Engel and others 2001; Fries and others 2001; Salinas and Sejnowski 2001; Bichot and others 2005; Taylor and others 2005; Womelsdorf and others 2006), sensorimotor integration (Murthy and Fetz 1992; Roelfsema and others 1997), or working memory (Tallon-Baudry and others 1998; Pesaran and others 2002).

Here we address the question if high-frequency population activity is monotonically related to feature intensity using whole-head MEG recordings in human subjects while they discriminate motion direction in dynamic random dot patterns. These stimuli are particularly well suited to investigate how the intensity of a specific sensory feature modulates neuronal activity. By varying the proportion of dynamic noise, the strength of visual motion can be parametrically manipulated while keeping other stimulus properties constant (Britten and others 1993; Bair and others 1994, 2001; Rees and others 2000).

Furthermore, the employed paradigm allows us to relate the present findings to other measures of neuronal activity. First, average firing rates in the macaque middle temporal area (MT) have been reported to exhibit an approximately linear dependency on the strength of visual motion in the same paradigm (Britten and others 1993). Second, by means of functional magnetic resonance imaging (fMRI), a linear dependency has also been demonstrated for the blood oxygen level–dependent (BOLD) response of the putative human homologue area MT+ and several other extrastriate cortical regions (Rees and others 2000).

Using the same parametric stimulus design as the previous studies, in combination with MEG, we investigated if frequency-specific neuronal activity is also systematically modulated by the strength of visual motion. Furthermore, we aimed at defining a functional frequency band, by testing in which frequency range such activity shows the strongest monotonic increase with visual motion strength. Finally, by combining MEG with distributed source reconstruction techniques (Van Veen and others 1997; Gross and others 2001), we investigated which cortical areas display such a modulation.

We report stimulus-induced high-frequency activity that shows the strongest increase with strength of visual motion in the high gamma band from about 60 to 100 Hz. We demonstrate that this modulation is consistently observed in all tested subjects and that it specifically occurs in several motion-responsive cortical regions.

Materials and Methods

Subjects, Stimuli, and Task

Seven subjects participated in the study (6 males and 1 female, mean age: 28.6 years, age range: 23–30 years). The study was conducted in accordance with the Declaration of Helsinki, approved by the local ethics committee, and informed consent was obtained from all subjects prior to the recordings. Two of the subjects are authors, whereas all other subjects were naive to the purpose of the experiment and were paid for their participation. All subjects were in good health, had no past history of psychiatric or neurological illness, and had normal or corrected-to-normal vision. All subjects participated in at least 6 recording sessions of a 2-alternative forced choice motion discrimination paradigm (subjects M.S. and T.H.D.: 7 sessions, remaining 5 subjects: 6

sessions), resulting in a minimum of 3600 recorded trials per subject. This large amount of trials was recorded to allow for a detailed single-subject analysis.

In each recording session, subjects performed 600 trials during which upward or downward motion had to be distinguished. Each trial was started by the onset of a red fixation cross on a uniform black background. After a random delay (1000–1500 ms), a dynamic random dot pattern of white dots on a black background was presented at 1 out of 6 levels of motion coherence (0%, 6.125%, 12.5%, 25%, 50%, and 100% motion coherence, 100 trials per level of motion coherence). On each trial, the coherent fraction of dots was moving in either upward or downward direction (50% upward motion and 50% downward motion). Dynamic random dot patterns were constructed using "random-position" noise according to a "different rule" (Scase and others 1996), as used previously (Britten and others 1993; Bair and others 1994, 2001; Bair and Koch 1996; Rees and others 2000). In short, for each frame, the level of motion coherence determined the fraction of dots that was displaced according to a common motion vector, whereas all other dots were displaced randomly (dot diameter: ~0.2 degrees, dot density: 1.7/degrees^2, motion speed: 11.5 degrees/s, local dot contrast: 100%). The set of coherently moving dots was randomly selected anew on each frame. That is, the coherent dots had limited "lifetime." All stimuli were confined to a circular central aperture in randomized sequence (aperture diameter: 43 degrees). The start position of dots was randomized uniformly over the entire aperture for each stimulus. Subjects were instructed to report the perceived direction of motion by a button press with either the left or the right index finger as accurately as possible but not to waste time until delivering the response. The stimulus–response mapping was counterbalanced across subjects. Stimuli were turned off immediately after the subject's response or 3 s after onset if no response was given until then. These stimuli of variable duration were used in order to minimize the effect of top–down factors on the recorded neuronal signals. By presenting the stimuli only until the subjects' response, it was ensured that subjects actively processed all stimuli during the used analysis interval (see below), irrespective of the level of motion coherence. Each trial was followed by a blank intertrial interval (1500 ms). All stimuli were constructed off-line using MATLAB (MathWorks Inc., Natick, MA), and stimulus presentation was controlled using the "Presentation" software (Neurobehavioral Systems, Albany, CA). All stimuli were presented via a mirror system on a back projection screen at a frame refresh rate of 60 Hz using a calibrated LCD projector positioned outside the recording chamber. The stimulus refresh rate induced narrow band signals that can be noted as sharp but weak 60-Hz bands in some of the presented spectra. As the spectral signature of the reported effects demonstrates that these are unrelated to the projector frequency, we did not make an attempt to remove or conceal these signal components.

Data Recording and Preprocessing

MEG was recorded continuously using a 151-channel whole-head system (Omega 2000, CTF Systems Inc., Port Coquitlam, Canada) in a magnetically shielded room. The electro-oculogram was recorded simultaneously for off-line artifact rejection. The head position relative to the MEG sensors was measured before and after each recording session. For all analyzed data sets, head displacements within a recording session were below 7 mm. Averaged across subjects, the standard deviation (SD) of head placements relative to the MEG dewar across recording sessions was 2.9 mm. MEG signals were low-pass filtered online (cutoff: 300 Hz) and recorded with a sampling rate of 1200 Hz.

Trials containing eyeblinks, saccades, muscle artifacts, and signal jumps were rejected off-line from further analysis using semiautomatic procedures. Line-signal removal was performed by selecting data segments of 10-s length from the continuously recorded data that contained the epochs of interest in the center. These epochs were Fourier transformed, the 50-, 100-, 150-, and 200- Hz Fourier components of the spectra were set to 0, and the time course of each epoch was finally reconstructed as the real part of the inverse Fourier transform of the corresponding spectrum. The epochs of interest were then cut out of these denoised 10-s data segments. This method exploits the fact that the line-signal artifact is of an almost perfectly constant frequency (below 0.1-Hz variability for the present data). Therefore, for the 10-s epoch, all the artifact energy is contained in the 50-Hz Fourier component and its harmonics. Subtracting these Fourier components on the segments of 10-s length results in a spectral notch of only 0.1-Hz width. As the actual spectral analyses used the multitaper method, with a spectral smoothing of more than 5 Hz, this notch typically becomes invisible. All preprocessed data were resampled at 600 Hz for data reduction.

T_1-weighted structural magnetic resonance imagings (MRIs) were recorded from all subjects. For the reconstruction of source-level activity, individual multisphere head models were derived from these structural MRIs. For the coregistration of source reconstructions with the individual cortical anatomy, cortical segmentation and surface reconstruction were performed on all individual structural MRIs using the BrainVoyager software (Brain Innovation B.V., Maastricht, The Netherlands).

Spectral Analysis and Response Quantification

All spectral analyses of the MEG data were performed using "multitaper" spectral estimates (Mitra and Pesaran 1999). In short, the data were multiplied by $N > 1$ orthogonal tapers and Fourier transformed, and the N spectral estimates were finally averaged. In case of power estimation, the spectra for each individual taper were magnitude squared after Fourier transformation. In case of cross-spectral density estimation for source reconstruction (see below), the autospectrum of each channel was multiplied with the complex conjugate spectra of all other channels for each individual taper before averaging across tapers. As data tapers, we used the leading $2TW-1$ prolate spheroidal (slepian) sequences, where T denotes the length of the tapers and W the half bandwidth. These tapers optimally concentrate the spectral energy of the signal over the desired half bandwidth W (Mitra and Pesaran 1999). All transformations to the frequency domain were performed on the single-trial level, and averaging across trials was finally performed in the frequency domain. Thus, all spectral estimates contained signal components phase locked and non phase locked to stimulus onset (Tallon-Baudry and Bertrand 1999).

We characterized spectral responses $\Delta R(f)$ as the percentage of change in signal amplitude at frequency f relative to the blank prestimulus baseline:

$$\Delta R(f) = \left(\frac{S(f) - B(f)}{B(f)}\right) 100\%, \qquad (1)$$

where $S(f)$ denotes the spectral amplitude in the temporal interval of interest and $B(f)$ denotes the spectral amplitude during the blank prestimulus baseline (500 ms before up to stimulus onset) averaged across all trials and levels of motion coherence for each recording session. Spectral amplitudes were computed as the square root of the spectral power estimate.

Sensor-Level Analysis

In order to characterize the temporal profile of spectral responses, we performed a time–frequency transformation of the MEG data using a sliding window multitaper analysis. A window of 200-ms length was shifted over the data with a window step size of 5 ms. Spectral smoothing of 10 Hz was achieved by using 3 slepian tapers. To derive the response according to equation (1), the baseline spectrum was estimated as the average spectrum of the time–frequency transform across the interval from 500 ms before up to stimulus onset. The lowest analyzed center frequency for all time–frequency analysis was 15 Hz.

To quantify the spectral profile of responses during the stimulus period, we computed response spectra for the stimulus period (100–500 ms past stimulus onset) and prestimulus baseline (500 ms before up to stimulus onset) using 8-Hz spectral smoothing and 5 slepian tapers. The lowest analyzed center frequency for all spectral analysis was 10 Hz. Restriction of the analysis window up to 500 ms past stimulus onset allowed us to use the same analysis window for all levels of motion coherence irrespective of the different response latencies. For all analyses on the sensor level, responses were averaged over those 30 sensors that, for each subject individually, showed the maximum response in the 60- to 100-Hz band from 100–500 ms past stimulus onset, averaging across all levels of motion coherence.

Source-Level Analysis

To estimate the spectral amplitude of responses at the cortical source level, we used an adaptive spatial filtering technique known as "linear beamforming" (Van Veen and others 1997; Gross and others 2001). In short, for each frequency f and source location r, a linear filtering matrix A was computed that passes activity from location r with unit gain while maximally suppressing activity from other sources. Formalization of these constraints yields the following solution:

$$A(r, f) = (L^T(r)C(f)^{-1}L(r))^{-1}L^T(r)C(f)^{-1}, \quad (2)$$

where $C(f)$ denotes the complex cross-spectral density matrix of all 151 simultaneously recorded MEG signals at frequency f. The columns of $L(r)$ contain the leadfield for 2 orthogonal tangential dipoles at location r. The complex cross-spectral density matrix $C(f)$ for the individual functional gamma band of each subject was computed independently for the stimulus (100–500 ms past stimulus onset) and baseline (500 ms before up to stimulus onset) period using multitaper spectral estimates with 20-Hz spectral smoothing and 15 slepian tapers. The leadfield matrix L was computed for each subject and recording session using a multisphere head model constructed from the individual structural MRIs and the measured head position relative to the MEG sensors. Based on the linear filtering matrix A, the power p at frequency f and location r is derived according to

$$p(r, f) = \lambda_1(A(r, f)C(f)A^{T*}(r, f)), \quad (3)$$

where λ_1 denotes the largest singular value operator that derives the power of a dipole in the dominant spatial direction. The linear beamformer exhibits a spatial bias, projecting more power to deeper sources. This bias is corrected for by normalizing the projected power with the projected noise (Van Veen and others 1997), which was computed according to equation (3), with replacement of the cross-spectral density matrix of the signals by the noise cross-spectral density matrix. We estimated the noise cross-spectral density matrix as the smallest singular value of the original cross-spectral density matrix times the identity matrix. As for all sensor-level analysis, source-level responses were characterized as the percentage of change in spectral amplitude during the stimulus period relative to the prestimulus baseline according to equation (1). The beamforming method cancels out distant and perfectly linearly correlated sources. However, experimental assessments of cortical correlation strength (Leopold and others 2003) as well as simulations (Van Veen and others 1997; Gross and others 2001; Sekihara and others 2002) show that this does not cause a problem in the physiological range of source correlation.

All source reconstructions were performed on a regular 3-dimensional grid of 6-mm resolution covering the entire cortical volume and were then linearly interpolated on a regular grid of 1-mm resolution. For each resulting voxel, the average responses and the modulation of response by motion coherence were analyzed using the method of sequential polynomial regression (see below). This analysis resulted in functional source-level images that were projected onto the individually reconstructed and Talairach-transformed cortical surfaces using BrainVoyager (Brain Innovation B.V.). Functional maps of the response modulation were thresholded at $P = 10^{-4}$ and $P = 10^{-7}$ for the individual data and group average, respectively. For the group average, source-level responses were pooled across all subjects after spatial normalization of all individual data to the International Consortium for Brain Mapping template (Montreal Neurological Institute, Montreal, Canada) based on the individual structural MRIs using the SPM2 toolbox (http://www.fil.ion.ucl.ac.uk/spm).

Analysis of Response Modulation

To statistically assess the modulation of responses by the strength of visual motion, we used sequential polynomial regression as described previously for the analysis of BOLD fMRI responses (Büchel and others 1998; Rees and others 2000). In short, the response y was modeled as a linear combination of basis functions of the stimulus variable c (motion coherence) equivalent to a polynomial expansion:

$$y = p_0 + p_1c^1 + p_2c^2 + \cdots + p_nc^n, \quad (4)$$

with p as polynomial coefficients. To independently assess the amount of accounted variance for each order of c, the different regressors of c were orthogonalized, and starting with the zero-order (constant) model, each model was sequentially tested in a serial hierarchical analysis based on F-statistics (Draper and Smith 1998). This analysis characterizes whether adding the next higher order model yields a significantly better description of the response than the respective lower order model. We tested models up to the order of 4. The same algorithm of sequential polynomial regression was used to characterize the spectrotemporal profile of response modulation, the spectral specificity of response modulation, the modulation of responses in the individual functional gamma band, and the spatial distribution of modulation at the cortical source level. In all single-subject analyses, the variance was assessed over recording sessions. For the analyses of population averages, the variance was assessed across subjects.

In order to derive a functional frequency band of visual motion, we determined for each subject a 40-Hz-wide frequency band in the range from 10 to 200 Hz that had the maximum average first-order (linear) coefficient of response modulation. This was achieved by convolving the spectrum of first-order polynomial coefficients with a 40-Hz-wide boxcar kernel and selection of the frequency of the global maximum of the resulting spectrum.

All analyses were performed in MATLAB (MathWorks Inc.) using the "FieldTrip" open source toolbox (http://www.ru.nl/fcdonders/fieldtrip) and with additional custom software.

Results

Psychophysics

The relationship between neuronal activity and visual motion strength was investigated in a 2-alternative forced choice motion direction discrimination paradigm (Fig. 1). With increasing motion coherence, the proportion of correctly performed trials increased monotonically, whereas response latency decreased (Fig. 1*C*). The mean threshold (82% correct performance) was at 13.9% motion coherence (standard error of the mean [SEM]: 2.6%). The mean response latency at threshold was 1.6 s (SEM: 0.1 s).

Visual Stimulation Induces Tonic High-Frequency Responses over Visual Cortex

In all subjects, visual stimuli induced a tonic increase in MEG signal amplitude in the high–gamma-frequency range (>50 Hz) at sensors overlying visual cortex (Fig. 2 and Supplementary Fig. 1). This tonic high-frequency response was complemented by a stable decrease in signal amplitude at frequencies below 30 Hz. These tonic visual responses were preceded by a transient response from about 50 to 100 ms at frequencies below 50 Hz. The sensor-level topography of the tonic high-frequency response induced by visual stimulation was similar across subjects, mainly confined to posterior sensors overlying the visual cortex. Therefore, for all subsequent sensor-level analyses and each individual subject, we averaged the responses over those 30 sensors with the strongest individual overall visual response, that is, those 30 sensors with the strongest 60- to 100-Hz response from 100 to 500 ms past stimulus onset averaged over all levels of motion coherence (Fig. 2*B*, see Supplementary Fig. 1 for all single-subject data).

To further analyze the spectral profile of the tonic response and its modulation by the strength of visual motion, we computed response spectra for the stimulus period (100–500 ms past stimulus onset) separately for each level of motion coherence (Fig. 3). Restricting the analysis up to 500 ms past stimulus onset ensured equal analysis windows for all levels of motion coherence irrespective of the different response latencies. These responses showed a consistent spectral profile across all subjects. In the frequency range below 30 Hz, visual

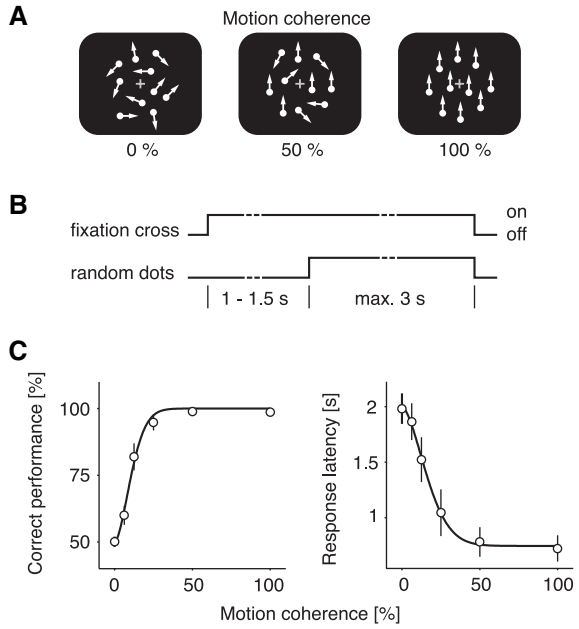

Figure 1. Experimental paradigm and psychophysics. (*A*) Schematic illustration of the dynamic random dot stimuli at 3 levels of motion coherence. At 0% motion coherence, all dots are randomly displaced from one frame to the next. At 50% motion coherence, half of the dots are displaced randomly between frames, whereas the other half moves in a common direction. At 100%, all dots share the same motion vector. Stimuli were presented at 6 logarithmically scaled levels of motion coherence ranging from 0% to 100% with either upward or downward coherent motion direction. (*B*) Time course of one trial. Trials start with onset of a fixation cross. After a random delay (1–1.5 s), dynamic random dot stimuli were displayed in a circular aperture until the subjects reported the perceived motion direction by pressing 1 of the 2 response keys. Stimulation was also terminated if no response was given within a 3-s time period. (*C*) Behavioral results averaged across all subjects. Correct performance (left panel) and response latencies (right panel) are plotted as a function of motion coherence. Continuous lines correspond to fitted Weibull functions.

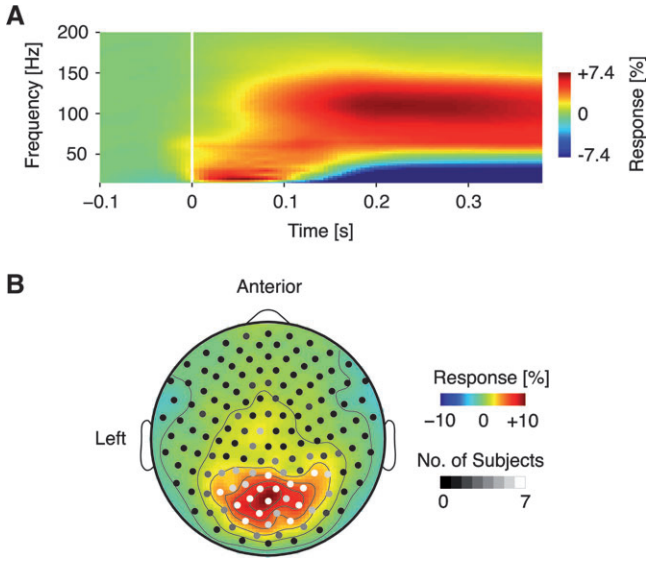

Figure 2. Visual stimulation induces sustained high-frequency responses. (*A*) Time–frequency representation of the response in MEG amplitude averaged across 30 sensors of interest and all stimuli and subjects. All responses are characterized as the percentage of change in signal amplitude relative to the blank prestimulus baseline (500 ms before up to stimulus onset). The white vertical line marks the time of stimulus onset. (*B*) Sensor-level topography of the tonic gamma-band response (60–100 Hz) during the stimulus interval (100–500 ms past stimulus onset) averaged across all stimuli and subjects. Sensor colors indicate the number of subjects for which each sensor was included in the sensor-level analysis.

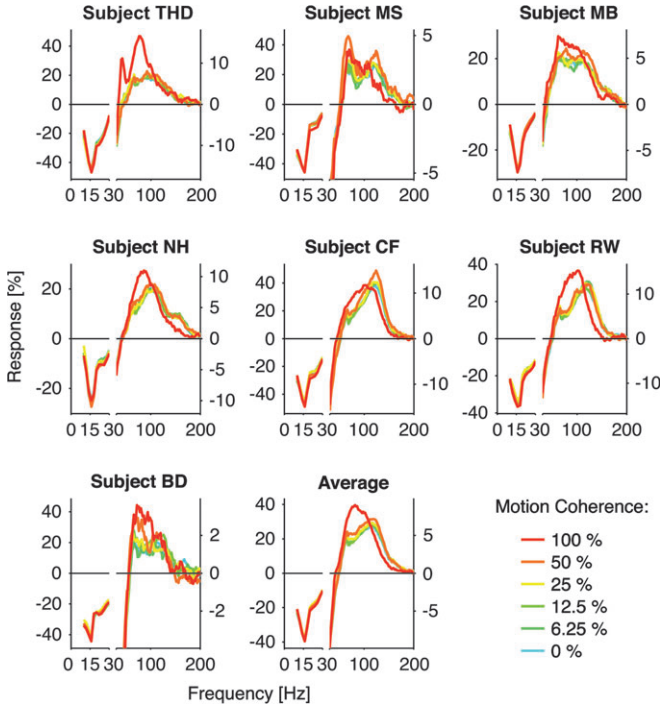

Figure 3. Spectral distribution of visual responses. The panels show the response in signal amplitude during the stimulus period (100–500 ms past stimulus onset) for each level of motion coherence. The figure displays the individual results for all recorded subjects and the population average (lower right panel). Note that because of the pronounced negative responses in the low-frequency range, responses are scaled separately for frequencies below and above 30 Hz.

stimulation led to a pronounced decrease in signal amplitude. This decrease showed 2 local minima at about 12 Hz (alpha band) and 25 Hz (beta band). At frequencies above 30 Hz, a broadband increase in signal amplitude was observed up to frequencies well above 100 Hz. In the frequency range from about 60 to 100 Hz, responses increased monotonically with strength of visual motion, whereas there was a decrease in responses to stimuli of the highest motion coherence at frequencies above about 110 Hz.

Responses Are Modulated by Visual Motion Strength

If frequency-specific activity plays a role in encoding visual motion, it should increase monotonically with visual motion strength. To determine the frequency ranges in which this criterion was met, we parametrically analyzed the motion-dependent response modulation by applying a sequential polynomial regression to the response at each single time and frequency (Büchel and others 1998; Draper and Smith 1998; Rees and others 2000). Each order of the polynomial model was then independently tested for a significant account of variance. Plotting the first- and second-order coefficients of the polynomial regression as a function of time and frequency depicts the full spectrotemporal evolution of the linear and quadratic modulation of neuronal activity by motion coherence (Fig. 4*A* and Supplementary Fig. 1). Across all subjects, this analysis revealed that the strongest linear increase (first-order coefficient) of activity with strength of visual motion indeed occurred in the frequency band from about 60 to 100 Hz, started 100 ms past stimulus onset and was then sustained. In the same temporal window, a significant positive linear

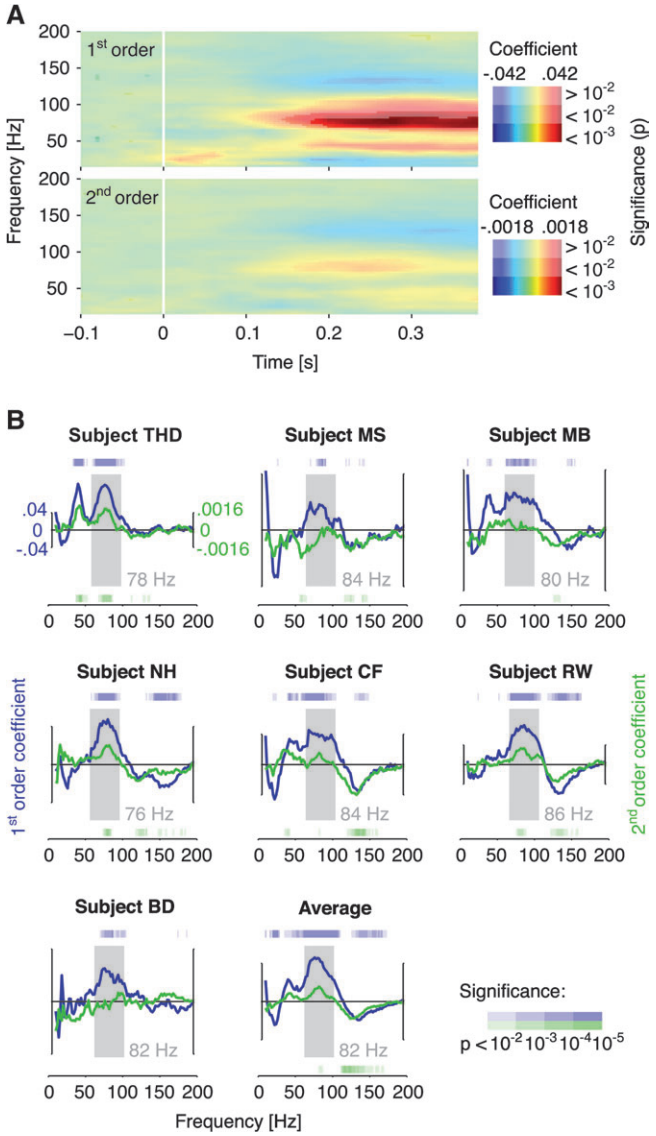

Figure 4. Spectral specificity of first- and second-order response modulations. (*A*) Time–frequency analysis of the first- (linear) and second-order (quadratic) modulation of responses by motion coherence. The 2 panels depict the spectrotemporal evolution of the corresponding polynomial coefficients. The statistical significance of modulations is indicated by the saturation of color scales. Vertical white lines mark stimulus onset. The panels show the average results across all subjects. (*B*) Panels display the spectral profile of response modulations during the stimulus period (100–500 ms past stimulus onset) for all individual subjects and the group average (lower right panel). Solid traces display the spectral distribution of first- (blue) and second-order (green) polynomial model coefficients. The frequency-dependent significance of these effects is indicated by the colored bars above and below the traces. Gray areas mark the individual 40-Hz-wide frequency bands with the strongest linear increase of activity with visual motion strength. Gray numbers denote the center frequencies of these bands.

modulation was also observed at about 40 Hz. A significant negative linear and quadratic (second-order coefficient) modulation was found at about 130 Hz.

To further investigate the spectral profile of these tonic response modulations in the stimulus period, we applied the same method of sequential polynomial regression to the average response at each single frequency in the window from 100–500 ms post stimulus onset. We visualized the spectral profile of the tonic response modulation by plotting the corresponding polynomial coefficients and their significance as a function of frequency (Fig. 4*B*). For all individual subjects as well as the group average, this analysis displayed a high intersubject reliability of the positive first-order modulation in the high gamma band from about 60 to 100 Hz. Three subjects displayed a significant positive second-order modulation in this frequency range. A smaller significant positive linear modulation in the lower gamma band at about 40 Hz was observed in 3 subjects. A significant negative first-order modulation in the low-frequency range (<30 Hz) was found in 3 subjects. In accordance with the frequency-dependent response functions (Fig. 3), a significant negative second-order effect was identified in the frequency range from about 100 to 150 Hz in 6 subjects.

Strongest Response Modulation Is Expressed in a Consistent High Gamma Band

Based on the above analysis, we next aimed at defining for each individual subject and for the average across all subjects a functional frequency band of visual motion. To this end, we determined which continuous 40-Hz-wide band displayed the maximum linear increase of activity with strength of visual motion (Fig. 4*B*, gray bands). Across all subjects, this analysis resulted in highly reliable frequency bands in the high gamma range with center frequencies at about 80 Hz (mean center frequency: 81 Hz, SD: 3.6 Hz).

To depict the modulation of responses by visual motion strength in these functional bands, we plotted the average response of activity across these frequency bands as a function of motion coherence (Fig. 5). In all investigated subjects, as well as in the grand average, gamma-band activity was strongly modulated by visual motion strength. To parametrically characterize the linearity of these response modulations, we again applied sequential polynomial regression. In all subjects as well as the group average, the linear (first order) model described the data significantly better than a constant model ($P < 10^{-4}$). Two subjects displayed a significant positive quadratic (second order) modulation ($P < 0.01$). Across all subjects, the mean additional variance accounted for by the quadratic compared with the linear model was 3%. Higher order models were not significant ($P > 0.05$). Whereas overall response magnitudes substantially differed across subjects, the magnitude of the modulation by motion strength showed a remarkable intersubject reliability. On average, the magnitude of response to stimuli of 100% motion coherence was about 1.7 times the magnitude of response to 0% motion coherence (mean response ratio: 1.71, SD: 0.26).

We conclude that the modulation of high-frequency responses by visual motion strength is very consistent across subjects. More specifically, the magnitude of response modulation as well as its spectral distribution is remarkably similar in all investigated subjects.

High- Frequency Activity Increases with Visual Motion Strength in Motion-Responsive Cortical Regions

The above analyses were based on the MEG spectral amplitude averaged across a group of 30 sensors overlying large portions of the occipital, parietal, and temporal cortex. In order to investigate the cortical specificity of the above-described modulations in the high gamma band, we next applied a distributed source reconstruction technique termed linear beamforming (Van Veen and others 1997; Gross and others 2001). In addition to the source-level analysis of the modulation of responses

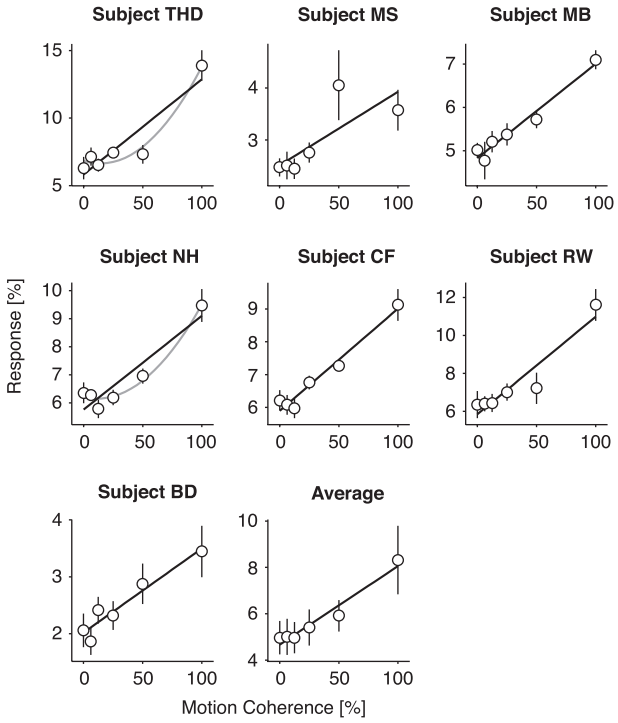

Figure 5. Modulation of responses in a functionally defined frequency band. The plots show the responses in the individually defined frequency bands during the stimulus period as a function of motion coherence. Results are displayed separately for each subject and for the average across all subjects (lower right panel). Solid lines correspond to fitted significant ($P < 0.01$) linear (black) and quadratic (gray) models.

by visual motion strength, we investigated the cortical distribution of the average visual responses across all levels of motion coherence. The latter analysis allowed us to validate the performance of the applied beamforming method against previous results that demonstrate strongest high-frequency responses near the calcarine sulcus (Hall and others 2005; Hoogenboom and others 2006). Moreover, it allowed us to investigate if the modulation of high-frequency activity is simply found in those regions with the strongest response or if it occurs specifically in regions involved in the processing of visual motion.

For each individual subject and level of motion coherence, cortical responses in the individually defined functional frequency band were reconstructed from the sensor-level data on a 6-mm grid covering the entire cortical volume. Sequential polynomial regression was then applied to the response at each cortical voxel. This analysis results in functional maps that depict the cortical distribution of the average gamma-band response across all levels of motion coherence (Fig. 6, red overlay, zero-order effect) and the positive linear modulation of gamma-band activity by visual motion (Fig. 6, blue overlay, first-order effect). In addition to the single-subject analysis, we computed the functional maps of the group average by pooling the responses across all subjects after spatial normalization of the individual source-level data to the Montreal Neurological Institute template brain (Fig. 6, lower right panel).

In all subjects, the global maximum of the visual gamma-band response across all levels of motion coherence was located near the occipital pole in pericalcarine cortex. This localization suggests a neural source in striate or early extrastriate visual cortex (V1, V2, V3) and accords well with previous reports (Hall and others 2005; Hoogenboom and others 2006). This localization of the average visual responses was contrasted by the pattern of regions that displayed a significant positive linear modulation of gamma-band activity by visual motion strength. Local maxima of this gamma-band modulation were located in the occipitoparietal and lateral occipitotemporal cortex (depicted as OP and LOT, respectively, in Fig. 6). All subjects as well as the group average showed a maximum in the occipitoparietal cortex. Six out of 7 subjects and the group average displayed a maximum in the lateral occipitotemporal cortex. The position of lateral occipitotemporal peaks with respect to the individual sulcal and gyral patterning corresponded to the typical location of human MT+, as defined by functional imaging: the junction of the ascending limb of the inferior temporal sulcus with the lateral occipital sulcus (Dumoulin and others 2000). Its average coordinates were also in accordance with those of fMRI-defined MT+ (average Talairach coordinates: $x = 46$, $y = -67$, $z = 0$, SD = 5, 5, 5, respectively) (Watson and others 1993; Tootell and others 1995; Dumoulin and others 2000).

Discussion

To characterize how the strength of visual motion modulates frequency-specific neuronal activity, we recorded MEG in human subjects performing a visual motion discrimination task. Our results show that activity in a high gamma band from about 60 to 100 Hz increases with strength of visual motion with a high reliability across individuals. Whereas strongest visual responses in this band originate from pericalcarine cortex, the strongest modulation of responses by visual motion strength was found in several motion-responsive regions remote from the pericalcarine cortex.

The stimulus-induced increase of gamma-band activity was accompanied by a pronounced decrease of low-frequency activity. Moreover, the positive correlation of gamma-band activity with visual motion strength was in some subjects complemented by a negative correlation in low-frequency ranges. This asymmetric behavior of activity in high- and low-frequency bands is consistent with previous experimental findings in visual cortex of cats, monkeys, and humans (Gray and others 1989; Roelfsema and others 1997; Tallon-Baudry and others 1998; Tallon-Baudry and Bertrand 1999; Fries and others 2001).

The large amount of data recorded in each subject ($\geq$3600 trials) allowed us to analyze the modulation of responses independently for each single subject. Remarkably, the magnitude of response modulation as well as the derived functional frequency band from about 60 to 100 Hz was highly consistent across all investigated subjects. The derived frequency range agrees well with several recent studies that describe stimulus-induced activity in the high gamma band in nonhuman primates (Eckhorn and others 1993; Logothetis and others 2001; Henrie and Shapley 2005) and humans (Crone and others 2001; Kaiser and others 2002; Edwards and others 2005; Hall and others 2005; Lachaux and others 2005; Tanji and others 2005; Hoogenboom and others 2006). Moreover, the frequency range derived here based on the modulation of responses by the intensity of a sensory feature accords well with previously defined bands based on the feature specificity of responses in visual cortex of alert cats and monkeys (Frien and others 2000; Siegel and König 2003; Kayser and König 2004). Thus, activity particularly in the high gamma band may be related to the processing and encoding of sensory information.

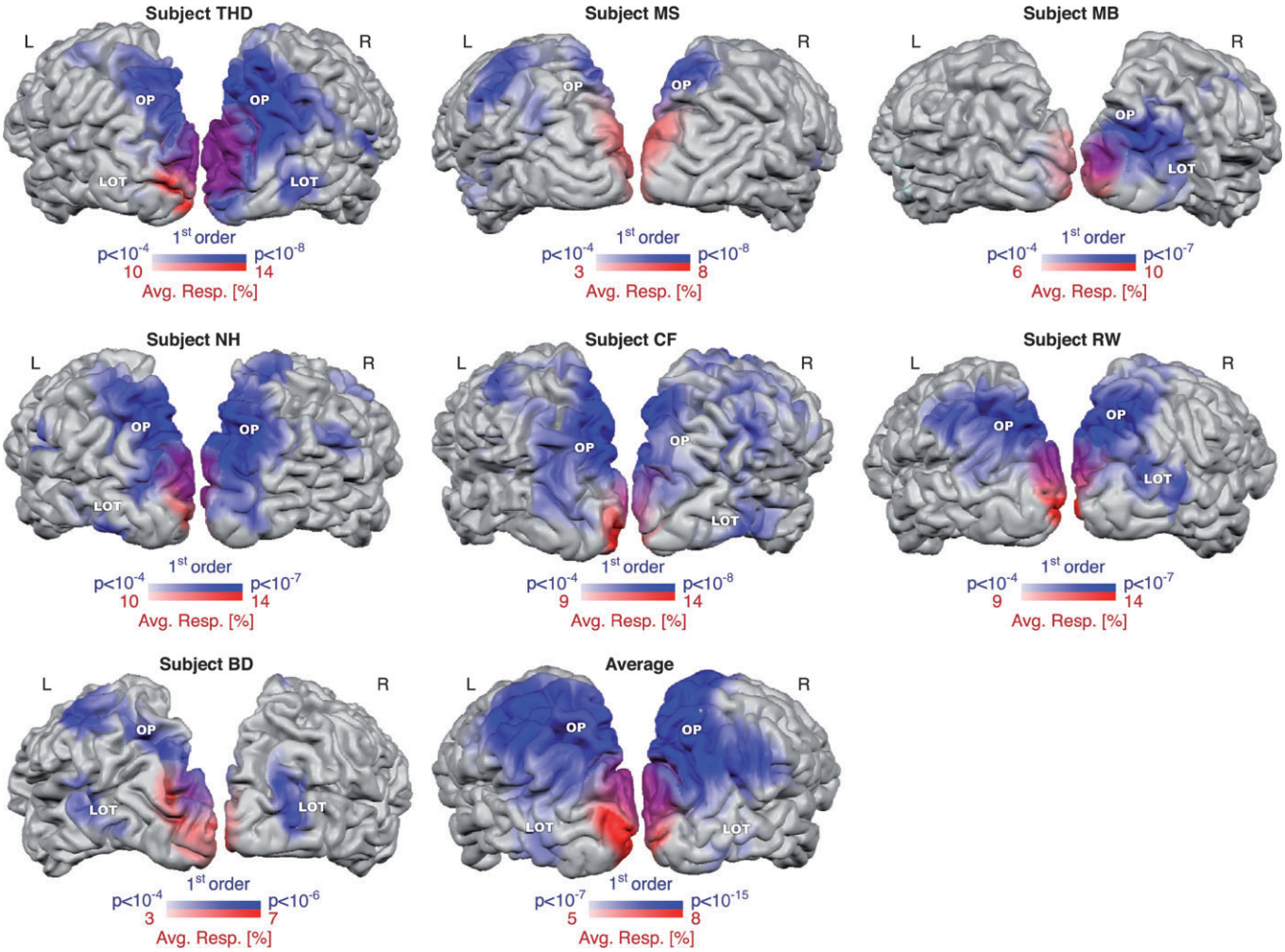

Figure 6. Spatial specificity of high-frequency responses and response modulations. The functional overlays display the spatial specificity of the average response in the individually defined functional frequency band across all levels of motion coherence (red overlay) and its linear modulation by visual motion strength (blue overlay). Functional maps are projected onto the reconstructed cortical surface of all individual subjects. Labels mark the local maxima of the linear modulation that have been assigned to the lateral occipitotemporal (LOT) and occipitoparietal (OP) cortex. The lower right panel displays the group average across all subjects.

As strength of visual motion increases with an increasing fraction of coherently moving dots, there is a concomitant decrease of stimulus transients due to random dot displacements. Recordings in primary visual cortex of alert cats suggest that feature selectivity and responses to stimulus transients prevail in different frequency ranges of the LFP, the former being prominent between 30 and 110 Hz and the latter dominating above 110 Hz (Siegel and König 2003; Kayser and König 2004). In accordance with these findings, the reduced responses to stimuli of the highest motion coherence at frequencies above 110 Hz could thus reflect a functional differentiation within the high-frequency range.

Employing the same paradigm as used here, a previous study has demonstrated a linear modulation of BOLD fMRI responses by visual motion strength in several extrastriate cortical regions and in particular in area MT+ (Rees and others 2000). We observed a corresponding modulation of gamma-band activity in a similar set of cortical regions including several extrastriate visual areas. Although the spatial resolution of MEG even in combination with adaptive distributed source reconstruction techniques is low compared with fMRI (Gross and others 2003; Liljestrom and others 2005), this set of areas accords roughly with areas found to be motion responsive by means of fMRI. Specifically, the regions characterized by the gamma-band modulation (occipitoparietal and lateral occipitotemporal cortex) have also been found to show an increase of the BOLD response with visual motion coherence (Rees and others 2000; Braddick and others 2001). Motion responsiveness is well documented in area MT+ in the lateral occipitotemporal cortex (Watson and others 1993; Tootell and others 1995; Rees and others 2000), in occipitoparietal regions, specifically in area V3A in the junction of the intraparietal with the transverse occipital sulcus (Tootell and others 1997), and in a not yet classified area located in the ventral part of the intraparietal sulcus (Sunaert and others 1999). The correspondence between feature-specific activity in the high gamma band demonstrated here and the corresponding modulations of BOLD responses accords well with recent invasive studies that demonstrate a close coupling of high-frequency LFP activity and the BOLD response (Logothetis and others 2001; Logothetis and Wandell 2004; Mukamel and others 2005; Niessing and others 2005).

Of particular interest in the present context is the prevalence of the gamma-band modulation in an area consistent with the human motion complex MT+ because previous studies investigating the temporal structure of spiking activity in the macaque analogue yielded substantially diverging results (Kreiter and Singer 1992, 1996; Bair and others 1994, 2001; de Oliveira and others 1997). Two studies had used moving bar stimuli and observed stimulus-induced synchronization of spiking activity in the gamma band that was correlated with stimulus properties (Kreiter and Singer 1992, 1996). By contrast, another study that employed drifting square wave gratings reported a stimulus-induced decrease in spike synchronization (de Oliveira and others 1997). Two other studies (Bair and others 1994, 2001) employed random dot stimuli, very similar to the ones used here, and found neither a modulation of the spectral signature of MT spiking activity nor a modulation of synchronization by visual motion strength. The discrepancy of the present results to these previous measurements could be due to several factors. Whereas typical extracellular recordings of spiking activity are weighted toward the output of the recorded units, the MEG signal measures, similar to the LFP, dendrosomatic currents, primarily reflect the neuronal input and local computation in a cortical region. Furthermore, the MEG signal reflects coordinated activity in large neuronal populations and may, therefore, be particularly well suited to detect changes in the frequency-specific neuronal synchronization.

Invasive recordings in macaque area MT have demonstrated a tight link between single-neuron firing rates and perception of visual motion (Britten and others 1996; Parker and Newsome 1998). In contrast, in the present data, the population average showed no increase of gamma-band activity over the first 3 levels of motion coherence, whereas motion direction discrimination performance increases steeply over this motion coherence range. This dissociation between psychophysical performance and the neuronal response suggests that gamma-band activity may not encode visual motion strength at very low levels of motion coherence and may thus not be the limiting factor for the motion discrimination task at hand. Moreover, the dissociation between psychophysical data and neuronal responses rules out that the observed modulations are simply caused by neural activity related to the behavioral response in combination with different response latencies. If such response-related activity caused the observed modulation, the increase of high-frequency activity with increasing motion coherence should exactly parallel the decrease in response latencies. In contrast, although response latencies are effectively identical for 50% and 100% motion coherence, there is a strong increase in high-frequency responses over that coherence range. Thus, the present modulations cannot be explained by response-related activity and variation of response latencies.

It is important to note that the reported frequency-specific modulation of MEG amplitude does not provide a direct measure of neural synchronization and could in principle reflect a change in the degree of neural synchronization and a change in synaptic activation levels. For the following reasons, the observed modulation of MEG amplitude most likely reflects both of these aspects: Several invasive recordings demonstrate that a spectrally specific enhancement of LFP amplitude is associated with increased synchronization of neuronal spiking and also enhanced spike-LFP synchronization in the same frequency range (Eckhorn and others 1988, 1993; Gray and Singer 1989; Herculano-Houzel and others 1999; Fries and others 2001; Siegel and König 2003). Moreover, a mere change of synaptic activation level without changes in the temporal patterning of activity (Britten and others 1993; Bair and others 1994) would result in a spectrally unspecific modulation of MEG amplitude, that is, similar modulation should be observed over the entire spectrum. In contrast, the present data show frequency-specific modulations in MEG amplitude with opposite effects in low- and high-frequency ranges. Taken together, these considerations suggest that the observed modulations reflect both a change in synaptic activation level and a frequency-specific change in the correlation structure of the contributing neural populations.

The increased spiking of neurons driven by a sensory feature might thus be accompanied by an increase in high-frequency synchronization among this neuronal population. In particular, in a regime of balanced excitation and inhibition (Salinas and Sejnowski 2000), this synchronization could enhance the impact of spiking activity on downstream neurons (König and others 1996; Engel and others 2001; Salinas and Sejnowski 2001; Azouz and Gray 2003; Sejnowski and Paulsen 2006). With increasing stimulus intensity, such stimulus-induced synchronization could dynamically enhance the gain of sensory representations. In contrast to a coding scheme based only on spike rate, this would provide a flexible and energy-efficient mechanism (Laughlin and Sejnowski 2003) to widen the dynamic range of neural representations as measured by their post-synaptic effect.

An interesting question is whether the response modulations described here are attributable to specific neuronal subpopulations as defined by their preferred direction of visual motion. Invasive recordings have demonstrated a strong correlation of neuronal high-frequency synchronization with the similarity of receptive field properties such as spatial overlap, preferred orientation, or preferred direction of motion (Gray and others 1989; Frien and Eckhorn 2000; Bair and others 2001; Palanca and DeAngelis 2005). The frequency-specific increase in activity measured at the population level by means of MEG may thus reflect an increase in synchronization specifically among the responsive subpopulation of neurons whose preferred direction of motion matches the visual stimulus. Whether such a population-specific increase in synchronization is paralleled by a decrease of synchronization among neurons with opposing direction preference, as has been demonstrated for MT firing rates (Britten and others 1993), remains to be studied in further investigations.

To conclude, our data demonstrate that the strength of visual motion correlates with gamma-band activity in the human visual motion pathway. This suggests that high-frequency activity in the human visual system may play a functional role in encoding the intensity of sensory features.

Supplementary Material

Supplementary figures can be found at: http://www.cercor.oxfordjournals.org/.

Notes

We thank Markus Bauer for helpful discussions. This study was supported by grants from the Deutsche Forschungsgemeinschaft (AKE), the European Commission (AKE), the Danish Research Council (RO), Netherlands Organization for Scientific Research (PF), Human Frontier Science Program (PF), and the Lungwitz-Foundation (AKE, MS, THD). *Conflict of Interest*: None declared.

Address correspondence to Markus Siegel, Department of Neurophysiology and Pathophysiology, Center of Experimental Medicine, University Medical Center Hamburg-Eppendorf, University of Hamburg, Martinistrasse 52, 20246 Hamburg, Germany. Email: m.siegel@uke.uni-hamburg.de.

References

Azouz R, Gray CM. 2003. Adaptive coincidence detection and dynamic gain control in visual cortical neurons in vivo. Neuron 37:513–523.

Bair W, Koch C. 1996. Temporal precision of spike trains in extrastriate cortex of the behaving macaque monkey. Neural Comput 8:1185–1202.

Bair W, Koch C, Newsome W, Britten K. 1994. Power spectrum analysis of bursting cells in area MT in the behaving monkey. J Neurosci 14:2870–2892.

Bair W, Zohary E, Newsome WT. 2001. Correlated firing in macaque visual area MT: time scales and relationship to behavior. J Neurosci 21:1676–1697.

Bichot NP, Rossi AF, Desimone R. 2005. Parallel and serial neural mechanisms for visual search in macaque area V4. Science 308:529–534.

Braddick OJ, O'Brien JM, Wattam-Bell J, Atkinson J, Hartley T, Turner R. 2001. Brain areas sensitive to coherent visual motion. Perception 30:61–72.

Britten KH, Newsome WT, Shadlen MN, Celebrini S, Movshon JA. 1996. A relationship between behavioral choice and the visual responses of neurons in macaque MT. Vis Neurosci 13:87–100.

Britten KH, Shadlen MN, Newsome WT, Movshon JA. 1993. Responses of neurons in macaque MT to stochastic motion signals. Vis Neurosci 10:1157–1169.

Büchel C, Holmes AP, Rees G, Friston KJ. 1998. Characterizing stimulus-response functions using nonlinear regressors in parametric fMRI experiments. Neuroimage 8:140–148.

Crone NE, Boatman D, Gordon B, Hao L. 2001. Induced electrocorticographic gamma activity during auditory perception. Brazier Award-winning article, 2001. Clin Neurophysiol 112:565–582.

de Oliveira SC, Thiele A, Hoffmann KP. 1997. Synchronization of neuronal activity during stimulus expectation in a direction discrimination task. J Neurosci 17:9248–9260.

Draper NR, Smith H. 1998. Applied regression analysis. New York: Wiley.

Dumoulin SO, Bittar RG, Kabani NJ, Baker CL Jr, Le Goualher G, Bruce Pike G, Evans AC. 2000. A new anatomical landmark for reliable identification of human area V5/MT: a quantitative analysis of sulcal patterning. Cereb Cortex 10:454–463.

Eckhorn R, Bauer R, Jordan W, Brosch M, Kruse W, Munk M, Reitboeck HJ. 1988. Coherent oscillations: a mechanism of feature linking in the visual cortex? Multiple electrode and correlation analyses in the cat. Biol Cybern 60:121–130.

Eckhorn R, Frien A, Bauer R, Woelbern T, Kehr H. 1993. High frequency (60–90 Hz) oscillations in primary visual cortex of awake monkey. Neuroreport 4:243–246.

Edwards E, Soltani M, Deouell LY, Berger MS, Knight RT. 2005. High gamma activity in response to deviant auditory stimuli recorded directly from human cortex. J Neurophysiol 94:4269–4280.

Engel AK, Fries P, Singer W. 2001. Dynamic predictions: oscillations and synchrony in top-down processing. Nat Rev Neurosci 2:704–716.

Frien A, Eckhorn R. 2000. Functional coupling shows stronger stimulus dependency for fast oscillations than for low-frequency components in striate cortex of awake monkey. Eur J Neurosci 12:1466–1478.

Frien A, Eckhorn R, Bauer R, Woelbern T, Gabriel A. 2000. Fast oscillations display sharper orientation tuning than slower components of the same recordings in striate cortex of the awake monkey. Eur J Neurosci 12:1453–1465.

Fries P, Reynolds JH, Rorie AE, Desimone R. 2001. Modulation of oscillatory neuronal synchronization by selective visual attention. Science 291:1560–1563.

Gray CM, König P, Engel AK, Singer W. 1989. Oscillatory responses in cat visual cortex exhibit inter-columnar synchronization which reflects global stimulus properties. Nature 338:334–337.

Gray CM, Singer W. 1989. Stimulus-specific neuronal oscillations in orientation columns of cat visual cortex. Proc Natl Acad Sci USA 86:1698–1702.

Gross J, Kujala J, Hamalainen M, Timmermann L, Schnitzler A, Salmelin R. 2001. Dynamic imaging of coherent sources: studying neural interactions in the human brain. Proc Natl Acad Sci USA 98:694–699.

Gross J, Timmermann L, Kujala J, Salmelin R, Schnitzler A. 2003. Properties of MEG tomographic maps obtained with spatial filtering. Neuroimage 19:1329–1336.

Gruber T, Muller MM, Keil A, Elbert T. 1999. Selective visual-spatial attention alters induced gamma band responses in the human EEG. Clin Neurophysiol 110:2074–2085.

Hall SD, Holliday IE, Hillebrand A, Singh KD, Furlong PL, Hadjipapas A, Barnes GR. 2005. The missing link: analogous human and primate cortical gamma oscillations. Neuroimage 26:13–17.

Henrie JA, Shapley R. 2005. LFP power spectra in V1 cortex: the graded effect of stimulus contrast. J Neurophysiol 94:479–490.

Herculano-Houzel S, Munk MH, Neuenschwander S, Singer W. 1999. Precisely synchronized oscillatory firing patterns require electroencephalographic activation. J Neurosci 19:3992–4010.

Hoogenboom N, Schoffelen JM, Oostenveld R, Parkes LM, Fries P. 2006. Localizing human visual gamma-band activity in frequency, time and space. Neuroimage 29:764–773.

Kaiser J, Lutzenberger W, Ackermann H, Birbaumer N. 2002. Dynamics of gamma-band activity induced by auditory pattern changes in humans. Cereb Cortex 12:212–221.

Kayser C, König P. 2004. Stimulus locking and feature selectivity prevail in complementary frequency ranges of V1 local field potentials. Eur J Neurosci 19:485–489.

König P, Engel AK, Singer W. 1996. Integrator or coincidence detector? The role of the cortical neuron revisited. Trends Neurosci 19:130–137.

Kreiter AK, Singer W. 1992. Oscillatory neuronal responses in the visual cortex of the awake macaque monkey. Eur J Neurosci 4:369–375.

Kreiter AK, Singer W. 1996. Stimulus-dependent synchronization of neuronal responses in the visual cortex of the awake macaque monkey. J Neurosci 16:2381–2396.

Lachaux JP, George N, Tallon-Baudry C, Martinerie J, Hugueville L, Minotti L, Kahane P, Renault B. 2005. The many faces of the gamma band response to complex visual stimuli. Neuroimage 25:491–501.

Laughlin SB, Sejnowski TJ. 2003. Communication in neuronal networks. Science 301:1870–1874.

Leopold DA, Murayama Y, Logothetis NK. 2003. Very slow activity fluctuations in monkey visual cortex: implications for functional brain imaging. Cereb Cortex 13:422–433.

Liljestrom M, Kujala J, Jensen O, Salmelin R. 2005. Neuromagnetic localization of rhythmic activity in the human brain: a comparison of three methods. Neuroimage 25:734.

Logothetis NK, Pauls J, Augath M, Trinath T, Oeltermann A. 2001. Neurophysiological investigation of the basis of the fMRI signal. Nature 412:150–157.

Logothetis NK, Wandell BA. 2004. Interpreting the BOLD signal. Annu Rev Physiol 66:735–769.

Lutzenberger W, Pulvermuller F, Elbert T, Birbaumer N. 1995. Visual stimulation alters local 40-Hz responses in humans: an EEG-study. Neurosci Lett 183:39–42.

Mitra PP, Pesaran B. 1999. Analysis of dynamic brain imaging data. Biophys J 76:691–708.

Mukamel R, Gelbard H, Arieli A, Hasson U, Fried I, Malach R. 2005. Coupling between neuronal firing, field potentials, and FMRI in human auditory cortex. Science 309:951–954.

Murthy VN, Fetz EE. 1992. Coherent 25- to 35-Hz oscillations in the sensorimotor cortex of awake behaving monkeys. Proc Natl Acad Sci USA 89:5670–5674.

Niebur E, Koch C. 1994. A model for the neuronal implementation of selective visual attention based on temporal correlation among neurons. J Comput Neurosci 1:141–158.

Niessing J, Ebisch B, Schmidt KE, Niessing M, Singer W, Galuske RA. 2005. Hemodynamic signals correlate tightly with synchronized gamma oscillations. Science 309:948–951.

Palanca BJ, DeAngelis GC. 2005. Does neuronal synchrony underlie visual feature grouping? Neuron 46:333–346.

Parker AJ, Newsome WT. 1998. Sense and the single neuron: probing the physiology of perception. Annu Rev Neurosci 21:227–277.

Pesaran B, Pezaris JS, Sahani M, Mitra PP, Andersen RA. 2002. Temporal structure in neuronal activity during working memory in macaque parietal cortex. Nat Neurosci 5:805–811.
Rees G, Friston K, Koch C. 2000. A direct quantitative relationship between the functional properties of human and macaque V5. Nat Neurosci 3:716–723.
Roelfsema PR, Engel AK, König P, Singer W. 1997. Visuomotor integration is associated with zero time-lag synchronization among cortical areas. Nature 385:157–161.
Salinas E, Sejnowski TJ. 2000. Impact of correlated synaptic input on output firing rate and variability in simple neuronal models. J Neurosci 20:6193–6209.
Salinas E, Sejnowski TJ. 2001. Correlated neuronal activity and the flow of neural information. Nat Rev Neurosci 2:539–550.
Scase MO, Braddick OJ, Raymond JE. 1996. What is noise for the motion system? Vision Res 36:2579–2586.
Sejnowski TJ, Paulsen O. 2006. Network oscillations: emerging computational principles. J Neurosci 26:1673–1676.
Sekihara K, Nagarajan SS, Poeppel D, Marantz A. 2002. Performance of an MEG adaptive-beamformer technique in the presence of correlated neural activities: effects on signal intensity and time-course estimates. IEEE Trans Biomed Eng 49:1534–1546.
Siegel M, König P. 2003. A functional gamma-band defined by stimulus-dependent synchronization in area 18 of awake behaving cats. J Neurosci 23:4251–4260.
Singer W, Gray CM. 1995. Visual feature integration and the temporal correlation hypothesis. Annu Rev Neurosci 18:555–586.
Steinmetz PN, Roy A, Fitzgerald PJ, Hsiao SS, Johnson KO, Niebur E. 2000. Attention modulates synchronized neuronal firing in primate somatosensory cortex. Nature 404:187–190.
Sunaert S, Van Hecke P, Marchal G, Orban GA. 1999. Motion-responsive regions of the human brain. Exp Brain Res 127:355–370.
Tallon-Baudry C, Bertrand O. 1999. Oscillatory gamma activity in humans and its role in object representation. Trends Cogn Sci 3:151–162.
Tallon-Baudry C, Bertrand O, Peronnet F, Pernier J. 1998. Induced gamma-band activity during the delay of a visual short-term memory task in humans. J Neurosci 18:4244–4254.
Tanji K, Suzuki K, Delorme A, Shamoto H, Nakasato N. 2005. High-frequency gamma-band activity in the basal temporal cortex during picture-naming and lexical-decision tasks. J Neurosci 25:3287–3293.
Taylor K, Mandon S, Freiwald WA, Kreiter AK. 2005. Coherent oscillatory activity in monkey area V4 predicts successful allocation of attention. Cereb Cortex 15:1424–1437.
Tootell RB, Mendola JD, Hadjikhani NK, Ledden PJ, Liu AK, Reppas JB, Sereno MI, Dale AM. 1997. Functional analysis of V3A and related areas in human visual cortex. J Neurosci 17:7060–7078.
Tootell RB, Reppas JB, Kwong KK, Malach R, Born RT, Brady TJ, Rosen BR, Belliveau JW. 1995. Functional analysis of human MT and related visual cortical areas using magnetic resonance imaging. J Neurosci 15:3215–3230.
Van Veen BD, van Drongelen W, Yuchtman M, Suzuki A. 1997. Localization of brain electrical activity via linearly constrained minimum variance spatial filtering. IEEE Trans Biomed Eng 44:867–880.
Watson JD, Myers R, Frackowiak RS, Hajnal JV, Woods RP, Mazziotta JC, Shipp S, Zeki S. 1993. Area V5 of the human brain: evidence from a combined study using positron emission tomography and magnetic resonance imaging. Cereb Cortex 3:79–94.
Womelsdorf T, Fries P, Mitra PP, Desimone R. 2006. Gamma-band synchronization in visual cortex predicts speed of change detection. Nature 439:733–736.